NJC

Light-driven Hydrogen Evolution with A Nickel Thiosemicarbazone Redox Catalyst Featuring Ni...H interactions under Basic Conditions

Journal:	*New Journal of Chemistry*
Manuscript ID:	NJ-ART-09-2014-001540.R1
Article Type:	Paper
Date Submitted by the Author:	15-Oct-2014

Complete List of Authors:	Jing, Xu; Dalian University of Technology, State Key Laboratory of Fine Chemicals Wu, Pengyan; DLUT, Liu, Xin; Dalian University of Technology, School of Chemistry Yang, Linlin; Dalian University of Technology, State Key Laboratory of Fine Chemicals He, Cheng; Dalian University of Technology, State Key Laboratory of Fine Chemicals Duan, Chunying; Dalian University of Technology,

Cite this: DOI: 10.1039/c0xx00000x

www.rsc.org/xxxxxx

ARTICLE TYPE

Light-driven Hydrogen Evolution with A Nickel Thiosemicarbazone Redox Catalyst Featuring Ni···H interactions under Basic Conditions

Xu Jing, Pengyan Wu, Xin Liu, Linlin Yang, Cheng He* and Chunying Duan

Received (in XXX, XXX) Xth XXXXXXXXX 20XX, Accepted Xth XXXXXXXXX 20XX

DOI: 10.1039/b000000x

The photocatalytic hydrogen evolution inspired by the highly evolved, finely tuned molecular photosynthetic systems in the nature represents an important process in sustainable solar energy conversion in the near future. By incorporating a phosphine donor within a thiosemicarbazone moiety, a new proton reduction catalyst Ni–**thioP**, featuring Ni···H interactions was synthesized and structurally characterized. Single crystal structure analysis revealed that the C–S, C–N and N–N bond lengths were all within the normal range of the single and double bonds, suggesting the extensive electron delocalization over the ligand skeleton. The presence of Ni···H interactions relative to the amide group coupled with the easy proton migration pathway involving thioamide/thiolate exchanging suggested that the thiosemicarbazone complexes could serve as promising candidates for proton reduction. Luminescence titrations exhibited that Ni–**thioP** served as efficiently luminescent quenchers for the photosensitizer **Fl**, providing the possibilities for the excited state of **Fl** to activate these catalysts for proton reduction. The direct generation of hydrogen was achieved by carrying out the photolysis of a solution containing fluorescein as the photosensitizer, triethylamine as the sacrificial and the redox catalysts. Ni–**thioP** exhibited high activity with a turnover number (TON) of 8000 moles of H_2 *per* mole of the catalyst after 24 hours and an initial TOF larger than 500 moles of H_2 *per* catalyst *per* hour. To further investigate the potential mechanism for proton reduction, calculations were also performed using density functional theory.

Introduction

Solar energy conversion of water into the environmentally clean fuel hydrogen offers one of the best long-term solutions for meeting energy requirements in the near future.[1-5] Inspired by the highly evolved, finely tuned molecular systems that exquisitely manage photon capture and conversion processes to drive oxygenic water-splitting,[6,7] current solar fuel research involves the developing new molecular systems. These systems comprises of a chromophore or photosensitizer for light absorption, a redox catalyst for H_2 evolution, an electron source for proton reduction.[8,9] Among the promising examples reported using transition metal complexes as redox catalysts, the highly active systems incorporating environmentally friendly organic dye as sensitizers (**PS**) are high desirable.[10,11] In particularly, redox catalysts that quench the excited state of organic dyes oxidatively in order to avoid the formation of unstable $\mathbf{PS}^-$ radical anions are immensely useful in the preparation of long-lived homogeneous systems.[12,13] Because the oxidative and reductive quenching processes usually coexisted in one system, the major challenge to create efficient catalysts goes beyond the achievement of an oxidative luminescence quenching, but includes the modification of the fast proton reduction process.

Thiosemicarbazones (**TSC**s) are strong chelating ligands for the transition metals that received considerable attention, because the transition metal complexes of them exhibit several pharmacological properties, depending on the parent aldehydes or ketones as well as the metal ions.[14,15] These complexes are also well known for the exhibiting of high stability in different kinds of biological media. Moreover, **TSC**s established a conventional proton migration path through the thiolate/thioamide resonance equilibrium.[16,17] Since both the proton transformation in the coordination catalysts and the interactions between the hydrogen atoms and the metal ions are the important factors influencing the proton reduction, the transition metal TSCs complexes might be promising candidates for the proton reduction, in the case of the redox potential of the species is well controlled.[18,19]

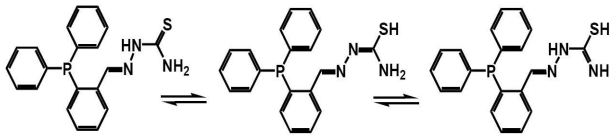

Scheme 1. Structure of H**thioP** with the thiolate/thioamide resonance tautomers.

Through incorporating a triphenylphosphine moiety as an additional donor to enhance the coordination ability of the metal centres (**Scheme 1**),[20,21] we reported resultant the thiosemicarbazone complex, Ni–**thioP** as an impressive catalyst for hydrogen production in a homogeneous system. As these nickel bis(diphosphine) complexes have been acted as effective reduction catalysts for electrochemical the photocatalytical

hydrogen production.[22,23] We envisioned that the *NSP* chelator would enhance the stability of these metal complexes and affords the nickel ions with suitable redox potentials for proton reduction, beneficial the system exhibiting highly catalytic efficiency for hydrogen evolution.[24,25] The strongly coordinated fields of the **NSP** chelator would be also conducive for the nickel centre coordinated in a suitable coordinated geometry, facilitating the coordination of water or H-atoms in axial position to accelerate the possible proton reduction reaction.[26,27] Our systems were incorporated by an environmentally friendly organic dye fluorescein(**Fl**) as the photosensitizer with triethylamine(**Et_3N**) as sacrificial electron donor to modify the photoinduced electron transfer pathways.[28]

Results and Discussion

2-(2-(diphenylphosphino)benzylidene)hydrazinecarbothioamide, HthioP, was synthesized by refluxing a methanol solution containing of thiosemicarbazide and 2-(diphenylphosphino)benzaldehyde for 4 hours. The resultant yield was 78%. When a chemical reaction between the ligand H**thioP** and $Ni(BF_4)_2.6H_2O$ was carried out in a methanol solution, the complex Ni–**thioP** was produced having a yield of *ca* 80%. Elemental analyses along with the powder X-ray diffraction analysis indicated the pure phase of its bulky sample. Single crystal X–ray structural analyses reveal a square planar coordination geometry of the Ni^{II} ion (**Figure 1**). The geometry is completed by a NSP chelator and a monosulphur donor from an oxidized ligand H**thioP**O. The oxidization process possibly occurred during the formation of crystals. Magnetic measurements indicated a diamagnetic behaviour of the bulk sample when the temperature was varied from 77 K to room temperature, thereby confirming the presence of Ni^{II} ion and its square planar coordination geometry in Ni–**thioP**. The Ni–S, Ni–N and Ni–P bond distances fall well within the separations in these related nickel thiosemicarbazones,[29,30] and nickel diphosphine complexes,[31] giving the possibility to establish the redox potential of the nickel ions. The intermediate between the formal single bonds and double bonds of the C–S, C–N and N–N bond distances demonstrates the electron delocalization within the ligand backbone. This implies that the protons attached to the ligand backbone are mobile.

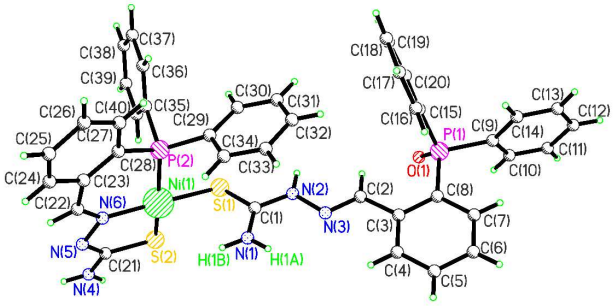

Figure 1 Structure of Ni–**thioP** showing the coordination geometry of nickel ion a. The anion and solvent molecules were omitted for clarity. Selected bond distances (Å): Ni(1)–S(1) 2.191(1), Ni(1)–S(2) 2.155(1), Ni(1)–P(2) 2.175(1), Ni(1)– N(6)1.890(3), C(1)– S(1) 1.716(4), C(21)–S(2) 1.733(4), N(1)–C(1) 1.304(4), N(2)–C(1) 1.328(5), N(2) –N(3) 1.388(4), N(3)–C(2) 1.274(5), N(4)–C(21) 1.338(5), N(5)–C21 1.306(5), N(5)–N(6) 1.414(4), N(6)–C(22) 1.298(5).

Furthermore, π–π stacking interactions were found between thiosemicarbazone skeleton of the monodentate ligand H**thioP**O (defined by atoms N(1), C(1), S(1), N(2) and N(3), mean deviation about 0.043Å) and one phenyl ring of another ligand (defined by atoms C(29), C(30), C(31), C(32), C(33) and C(34), mean deviation about 0.005Å). The dihedral angle between the two planes was 12.5(6)°, whereas the plane to plane separation was about 3.43 Å. One of the amide hydrogen atoms was positioned on the vertical position of the coordinated plane. The Ni(1)···H(1B) separation was about 2.82 Å and the Ni···H–N angle was 156°. The potential interactions relative to the hydrogen atom of theamide group thus gave the possibility of Ni–**thioP** to exhibit the fast proton reduction in the lower valence form of the nickel atom.[32,33]

When we referred to the cyclic voltammograms of Ni–**thioP**, it exhibited one pseudo-reversible redox peak at –0.78 V (*vs* Ag/AgCl), which could be attributed to the overlapping of $Ni^{II/I}/Ni^{I/0}$ (**Figure 2**). With the addition of H**NEt_3**Cl to the reacting species, a new peak near to the redox potential was appeared in the spectrum. Meanwhile, when the concentration of **Et_3NH^+** is increased at this stage, the height of the new wave also increased. Moreover, the catalytic wave shifted simultaneously toward more negative potentials as its height increased. The new wave is reasonably assignable to the typical proton reduction, indicating that Ni–**thioP** is able to reduce proton through a catalytic process. Ni–**thioP** was also an efficient quencher for the photosensitizer **Fl**; the titration curve followed the linear Stern–Volmer behaviour with the constant $k_{SV} = 1.47 \times 10^4\ M^{-1}$. The quenching behaviour is also assignable to the photoinduced electron transfer process from the excited state of **Fl*** to Ni–**thioP**. This indicates that **Fl** has the capability to activate Ni–**thioP** for proton reduction in the solution.[34,35]

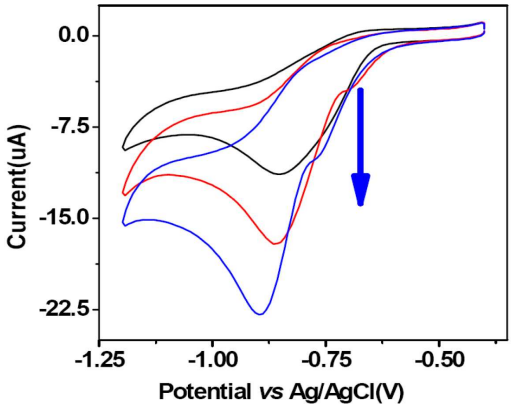

Figure 2. Cyclic Voltammogram of Ni-thiop (1 mM) (black line) in CH_3CN with 0.1 M $TBAPF_6$ upon addition of Et_3NHCl with concentrations of 5.0 mM (red line) and 10.0 mM (blue line), respectively. Scan Rate: 100 mV/s.

The generation of hydrogen was brought about by carrying out the photolysis of a solution of **Fl** and Ni–**thioP** in a 1:1 EtOH /H_2O solvent mixture containing **NEt_3** at room temperature. The pH of the reaction mixture was maintained at 12.5 throughout the process. The system exhibited excellent activity with the turnover number was about 8000 moles of H_2 *per* mole of the catalyst after 24 hours and initial TOF was greater than 500 moles of H_2 *per* catalyst *per* hour, when the concentrations of Ni–**thioP** and **Fl** were 10.0 μM and 4.0 mM, respectively. Since thiosemicarbazones constitute a large family of bioactive systems, our

design strategy could be extensively extended to obtain highly efficient catalysts.[36,37] Using a solution containing fixed concentration of **Fl** (2 mM), the initial rates for the hydrogen generation showed a first-order dependence on the concentration of Ni–**thioP** (**Figure 3**). When the concentration of **Fl** varies, the TOF reached the platform value at 3.0 mM. The light-induced hydrogen production also depends on the concentration of sacrificial reagent: the optimal concentration is 5%, characterized with a decrease in activity at both lower and higher concentration (**Figure 4**).

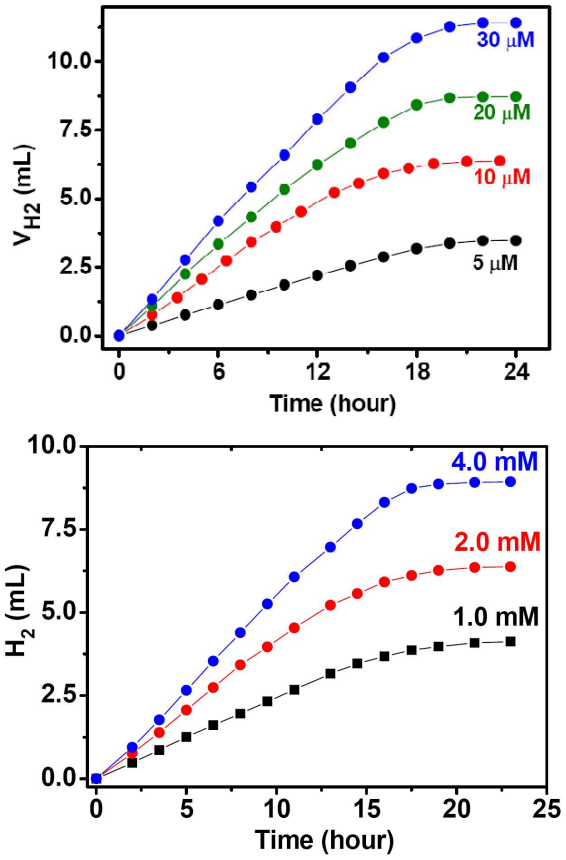

Figure 3 Top picture: Photocatalytic hydrogen evolution of system containing 2.0 mM Fl, 5% NEt3 (in v/v) with concentration of Ni–**thioP** at 5.0 μM (black), 10.0 μM (red), 20.0 μM (green), 30.0 μM (blue line), respectively. Bottom One: Photocatalytic hydrogen evolution of the systems containing 10.0 μM Ni–**thioP**, 5% NEt_3 (in v/v) with the concentration of Fl, at 1.0 mM (black), 2.0 mM (red) and 4.0 μM (blue line), respectively.

As illustrated by the catalytic wave at the potential of the Ni–**thioP**$^{+}$/Ni–t**hioP**, the reduction to the complex first occurs in the metal center. While the oxidation state of nickel in the compound Ni–**thioP** can be formally assigned as Ni^{I}, the nature of the thiosemicarbazone ligand increases the possibility of a direct interaction between the amide hydrogen and the nickel center.[23] Accordingly, an electron-rich $nickel^{II}$ intermediate is thought to proceed through the protonation of Ni^{I} center, resulting in the formation of a Ni^{II}-H intermediate. This indicates that direct metal–H interaction is able to assist the proton reduction process in compound Ni–**thioP.** The protonation of the anionic thiosemicarbazone moiety results in the formation of the ligand H**thioP**, reminiscent of the accepted mechanism for the nickel bis(diphosphine) catalyst[38,39] and the iron-only hydrogenase for H_2 generation.[40,41] Ni–**thioP** is a representative example that could be used to elucidate how a stable photosynthetic system developed with organic dyes.[42,43]

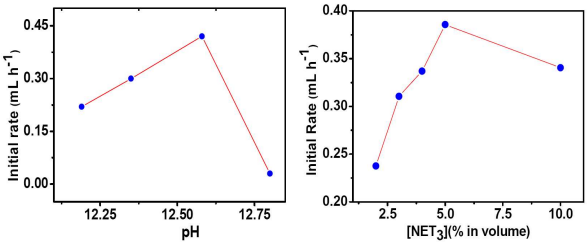

Figure 4 The initial rates of H2 production in EtOH/H_2O (1:1) of systems containing Ni-**thiop** (10.0 μM), Fl (2.0 mM) and 5% of NEt3 with the different pH value (Left Picture) and of systems containing Ni-thiop (10.0 μM), Fl (2.0 mM) at pH 12.5 with the different concentration of NEt_3 (right one).

Theoretical calculation was performed using density functional theory, and the values obtained from the calculations were to investigate the aforementioned reaction mechanism for the proton reduction. The experimental structure of compound Ni–thioP was well-reproduced according to the DFT calculations at ωB97XD/ 6-31+g(d,p)//LANL2DZ level.[44,45] The calculated bond lengths are 2.27, 2.20, 2.23, 1.93, 1.73 and 1.75Å for Ni(1)–S(1), Ni(1)–S(2), Ni(1)–P(2), Ni(1)–N(6), C(1)–S(1) and C(21)–S(2), respectively. It is worthwhile to note that the long-distance Ni···H interaction relative to the proton of the amide group was reproduced as 2.76 Å, thereby proving the possibility that the proton transfer in this direction to reduce the proton to its low-valence form. While analyzing the frontier orbitals of Ni–**thioP,** we found that as d_z^2 orbital of the Ni^{II} centre is occupied in the 4-coordinated planar structure, the HOMO is contributed by the interaction of Ni^{II} d_{xy} orbital and the ligand, whereas the LUMO is contributed mainly by the Ni^{II} $d_{x^2-y^2}$

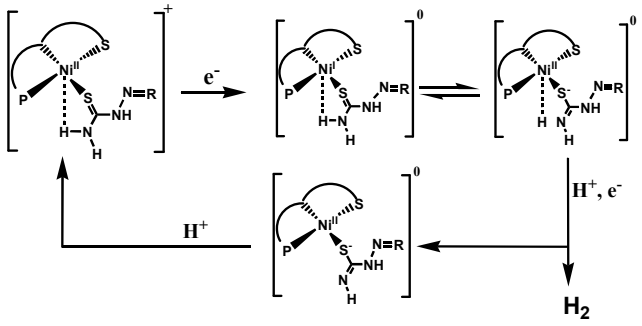

Scheme 2. Possible structures of nickel species involved in proton reduction for the hydrogen formation.

According to the hydrogen evolution mechanism proposed by DuBios et al, an electron transfer to the complex is required to initiate the proton reduction.[42,43] The LUMO contributed by Ni^{II} d_{x2-y2} acts as the receptor of the electron, and this finding is proved by the calculated spin density that is mainly localized on the central Ni atom. The Ni–S(1) is elongated by 0.47 Å and the Ni–N(6) is also prolonged to 2.11 Å. As mentioned previously, Ni···H bond is shortened to 2.73 Å, whereas the Ni···H bonding

COOP population is strongly enhanced around the HOMO, suggesting the promoted interaction between the proton of amide group and the reduced Ni centre. It should be noted that after charge transfer, the Ni centre is positioned as an additional negatively charged species, whereas the proton associated with the amide group is slightly positively charged according to the Mulliken population analysis.Additionally, the electrostatic interaction may additionally contribute to the driving force for proton transfer and subsequent reduction.

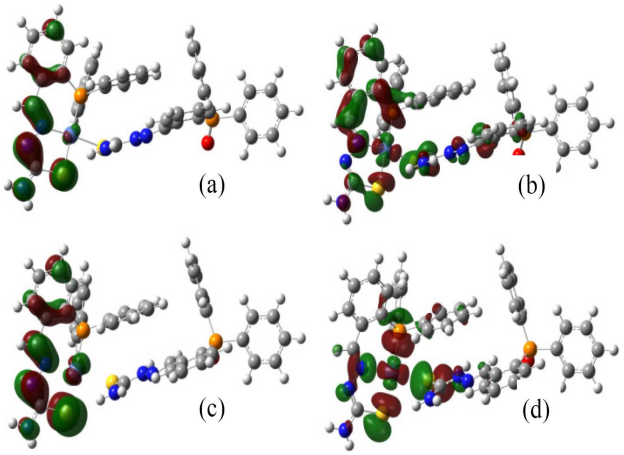

Figure 4 HOMO(a) and LUMO (b) of Ni–**thioP**, and HOMO-1(c) and HOMO (d) of the reduced Ni–**thioP**, The isovalue is 0.03 a.u. for orbitals.

The proton transfer and reduction was investigated over both the as synthesized Ni–**thioP** and its reduced form. To conduct a comprehensive investigation, we considered all the possible H trapping centres, including the Ni–S, Ni–P and Ni–N bonds. These trapping centres have been included in previously discussions elucidating hydrogen evolution using nanoparticles of transition metal sulphides and phosphides (**Figure 4**).[46,47] But with reference to Ni–**thioP,** the proton was recaptured by the amide group in each of these cases. This implies that the energy barrier for such a process is not thermodynamically preferable. After charge transfer, the complex molecule of Ni–**thioP** undergoes a free energy change was about 94.12 kcal/mol. The reduced proton adsorption over the Ni centre was observed, and the corresponding free energy change was calculated to be 45.18 kcal/ mol. In previous studies, it has been reported that the free energy change of about 54.4 kcal/mol occurs for the proton reduction over a $Ni(depp)_2^{2+}$ hydride donor; the free energy change at this level further supports the high efficiency of the reduced Ni–**thioP** in proton reduction.[41,42]

The reaction of the ligand H**thioP** and $Co(BF_4)_2{\cdot}6H_2O$ in a methanol solution led to the formation of another complex Co–**thioP** in a yield of about 75%. Elemental analyses along with powder X-ray analysis indicated the pure phase of its bulky sample. Single crystal structural analysis revealed the presence of a +1 charged cation and a BF_4^- anion in an asymmetric unit. The cobalt centre was octahedrally coordinated by two SNP chelators that originated from two different ligands, respectively (**Figure 5**). The two ligands coordinated to a cobalt atom in a *mer* configuration with pairs of S atoms and P atoms, each bearing a *cis* relationship. The two thiosemicarbazone N atoms were *trans* to each other, as found in the related cobalt thiosemicarbazone complexes.[48,49] The C–S, C–N and N–N bond distances were all within the normal ranges of single and double bonds, indicating the extensive electron delocalization over the ligand skeleton.[50,51] Consequently, the proton would easily immigrate onto a suitable position during the proton reduction process, beneficial to the high efficiency of the catalytic system.[52] And the Co–**thioP** was described as a reference of Ni–**thioP** on the hydrogen evolution.

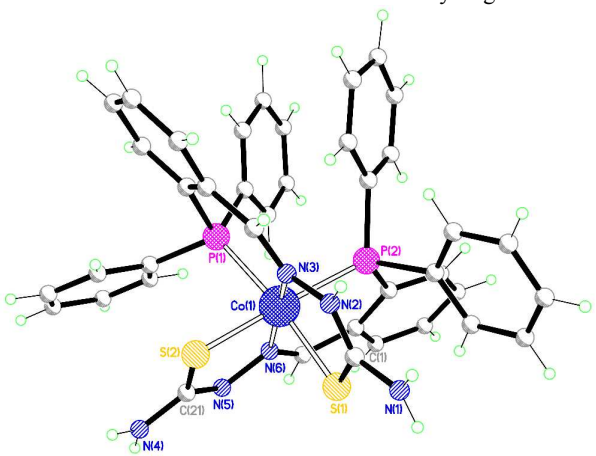

Figure 5. Molecular structure of Co–**thioP** showing the coordinated geometry of the cobalt ion. Anions and the solvent molecules were omitted for clarity. Selected bond distances (Å): Co(1)–S(1) 2.244(1), Co(1)–S(2) 2.238(1), Co(1)–P(1) 2.272(1), Co(1)–P(2) 2.287(1), Co(1)–N(3) 1.929(3), Co(1)–N(6) 1.938(4) C(1)–S(1) 1.720(5), N(1)–C(1) 1.304(4), N(2)–C(1) 1.328(5), N(2)–N(3) 1.388(4), N(3)–C(2) 1.274(5), C(21)–S(2) 1.715 (5), N(4)–C(21) 1.338(5), N(5)–C(21) 1.306(5), N(6)–C(22) 1.298(5), N(5)–N(6) 1.414(4).

Electrospray ionization mass spectrum exhibits an intense peak at *m/z* = 783.18, assignable to Co(**thioP**)(H**thioP**)$^+$, demonstrating the formation of Co–**thioP** in solution. Cyclic voltammogram of Co–**thioP** in an acetontrile solution exhibits a pseudoreversible Co^{II}/Co^{I} redox process at -0.46V (*vs*. Ag/AgCl). Addition of $\mathbf{Et_3NH^+}$ triggers the appearance of a new cathodic wave near the Co^{II}/Co^{I} response. Increasing the concentration of $\mathbf{Et_3NH^+}$ raises the height of the new wave and shifts it to more negative potentials (**Figure 6**). This wave is attributed to the proton reduction process, indicating that Co–**thioP** is able to reduce the proton.[53,54] Co–**thioP** also serves as an efficient quencher for the photosensitizer fluorescein **Fl**. When Co–**thioP** was added to the 1:1 EtOH/H_2O solution of fluorescein (10 μM), emission quenching at pH 12.5 were observed. The titration curve follows the Stern–Volmer behaviour with quenching constant k_{SV} of 6.0×10^3 M^{-1}. The quenching is attributed to photoinduced electron transfer from the excited state of **Fl*** to Co–**thioP**, providing the possibilities for the excited state **Fl** to activate Co–**thioP** for the proton reduction.

Photolysis of a solution of **F1** (2.0 mM) and Co–**thioP** (10 μM) was displayed in a solvent mixture containing triethylamine (**Et_3N**) (10% in volume, 0.72 M) in a 1:1 H_2O/EtOH mixture solvent. The volume of H_2 was quantified at the end of the photolysis by gas chromatographic analysis of the headspace gases.[55,56] It was found that the higher efficiency could be achieved at pH 11.5–13.0. Decreasing pH values from 12.5 to 10.0 resulted in both a lower initial rate and shorter system

longevity for hydrogen evolution (**Figure 7**). The decrease of the efficiency at higher pH values was likely due to the lower proton concentration in solution. Control experiments of the systems with the absence of any one species of Co–**thioP**, **Fl** or **Et_3N** hardly yielded any observable amount of H_2 demonstrating that all of three species are essential for the hydrogen generation. These artificial photosynthetic systems could not work well in the absence of the light, either.

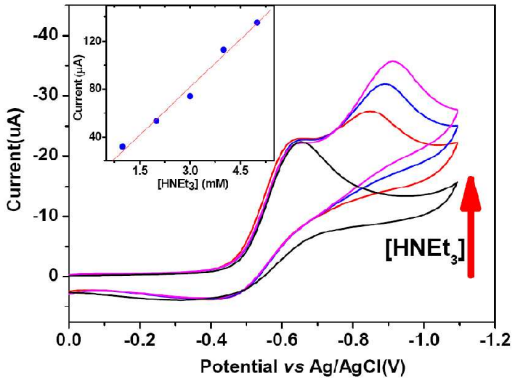

Figure 6. CV of Co–**thioP** (1.0 mM) and TBA·PF_6 (0.10 M) in an acetontrile solution (black line) upon addition of $HNEt_3Cl$ with concentrations of 2.0 mM (red line), 4.0 mM (blue line) and 6.0 mM (pink line) respectively. Scan rate of 100 mV/s; the insert showing the i_c vs [$HNEt_3$].

When fixed concentrations of **Fl** and **NEt_3** are used in the reaction mixture, the initial rate of hydrogen generation has a first-order dependence on the concentration of Co–**thioP** in the range of 5.0 μM to 30.0 μM (**Figure 5**). The initial turnover frequency (**TOF**) calculated is about 200 moles H_2 per mole catalyst per hour, while the turnover number (**TON**) is 2000 moles H_2 per mole of catalyst. The values are comparable to the highest one reported in **Fl**/cobalt systems.[57,58] At higher catalyst concentrations ([Co–**thioP**] > 30 μM), the **TON** does not scale linearly with catalyst concentration although a larger amount of hydrogen is evolved.

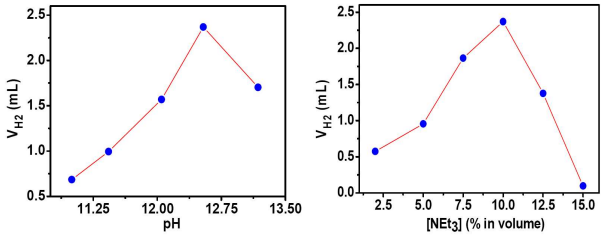

Figure 7. Left Picture: Photocatalytic hydrogen evolution of the systems containing Co-**thiop** (10.0 μM), **Fl** (2.0 mM), **Et_3N** (10% v/v) at different pH values; and Right One: Photocatalytic hydrogen evolution of the systems containing Co-**thiop** (10.0 μM), **Fl** (2.0 mM) at pH 12.5 with various Et3N concentration in 1:1 EtOH/H_2O, respectively.

When the concentrations of **Fl** varied, the **TOF** and **TON** attain the platform value at 3.0 mM (**Figure 8u**). After attainment of the platform value, further addition of **Fl** causes negligible TON enhancement corresponding to the catalyst. Control experiments through adding of isolated **Fl** (2.0 mM), Co–**thioP** (10.0 μM) or **NEt_3** (10% in volume) to a reaction flask after cessation of the hydrogen evolution, did not give further hydrogen evolution. And the addition of two of the three components of the homogeneous system, except that **Fl** (2.0 mM) and Co–**thioP** (10.0 μM), could not give any further hydrogen evolution, either.

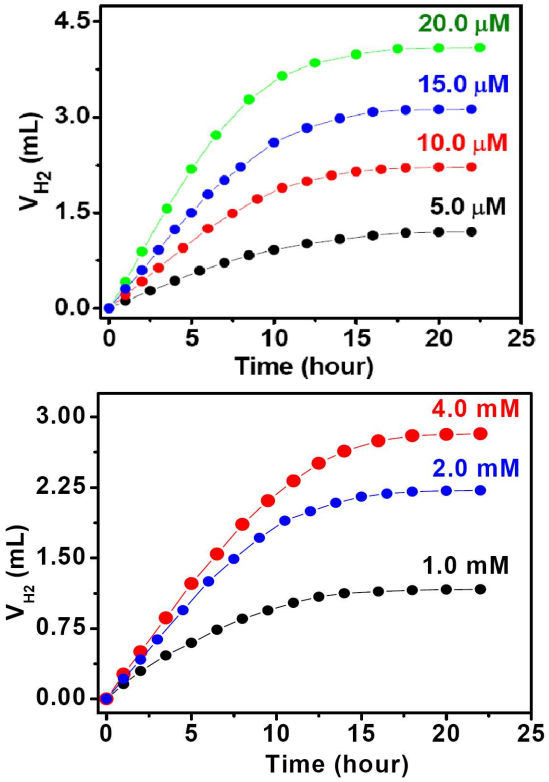

Figure 8 Photocatalytic H_2 evolution of the systems (Top picture) containing 2.0 mM **Fl**, 10% **NEt_3** (v/v) with the concentration of Co–**thioP** at 5.0 μM (black line), 10.0 μM (red line), 15.0 μM (blue line) and 20.0μM (green line), respectively. And of the systems containing 10.0μM Co– **thioP**, 10% **NEt_3** (v/v) with the concentration of **Fl**, at 1.0 mM (black), 2.0 mM (blue) and 4.0 μM (red line), respectively (Bottom One).

The efficiency of the visible light induced hydrogen evolution also depends on the concentration of sacrificial reagent **NEt_3**. The optimal concentration is 10 %, with a decrease in activity at both lower and higher concentration. While the Stern–Volmer quenching constant of Co–**thioP** is about 10^4 times greater than that of **NEt_3**(0.44 M^{-1}), a reduction quenching by **NEt_3** dominated the artificial photosynthetic system. This could be attributed to the fact that the concentration of **NEt_3**, (10%, 0.72 M) was much higher than that of Co–**thioP** in the reaction mixture. A potential oxidative quenching was hypothesized with a higher concentration of redox catalyst Co–**thioP** (40 μM) and lower concentration of **NEt_3** (1.0%, 72 mM).[59,60] Experimental results suggested that the hypothesized system indeed has a prolonged lifetime, however, the **TOF** was reduced to 30 moles H_2 per mole catalyst per hour.

Conclusions

New metal thiosemicarbazone complexes containing phosphine donors were achieved as proton reduction catalysts for light driven hydrogen evolution in a homogeneous environment with fluorescein as the photosensitizer. The oxidative quenching mechanism toward fluorescein by Ni–t**hioP** was suitably

modified to prolong the life thime of the light-driven hydrogen evolution systems, by carefully adjusting the redox potentials of the catalysts, the concentrations of the catalysts and the sacrificial electron donors. The intramolecular Ni···H interactions coupled with the fast proton immigration pathways indicated that thiosemicarbazone complexes served as promising candidates for proton reduction. The photocatalytic systems exhibited excellent activity with a turnover number (**TON**) of 8000 moles of H_2 *per* mole of the catalyst after 24 hours and an initial TOF larger than 500 moles of H_2 *per* catalyst *per* hour. As the oxidative and reductive quenching processes coexisted within the present system, the major challenge to achieve efficient catalysts goes beyond the achieving of an oxidative luminescence quencher, but includes the modifying of the hydrogen reduction process

Experimental Section

Material and Methods.

All chemicals were of reagent grade quality obtained from comer-cial sources and used without further purification. The elemental analyses of C, H and N were performed on a Vario EL III elemental analyzer. ^{1}H NMR spectra were measured on a Varian INOVA 400 M spectrometer. ESI mass spectra were carried out on a HPLC-Q-Tof MS spectrometer using methanol as mobile phase. Uv-vis spectra were measured on a HP 8453 spectrometer.

Solution fluorescent spectra were measured on JASCO FP-6500. Both the excitation and emission slit widths were 2 nm and the emission were recorded with the excitation at 460nm. The high concentrations of the stock solution of the organic dye and the redox catalysts (1.0×10^{-2} M) were prepared in N,N'-dimethylformamide. Before spectroscopic measurements, the solution of fluorescein (10 μM) was freshly prepared by diluting the high concentration of stock solution with a EtOH/water (1:1) solutions. 2 mL host solution was placed into a test tube, adding an appropriate aloquto of each rodoxcatalyst stock into the host solution, excitation at 460 nm.

Electrochemical measurements were carried under nitrogen at room temperature, performed on ZAHNER ENNIUM Electro-chemical Workstation with a conventional three-electrode system with a homemade Ag/AgCl electrode as a reference electrode, a platinum wire with 0.5 mM diameter as a counter electrode, and glassy carbon electrode as a working electrode. Cyclic voltamo-grams with displayed with the concentrations ca. 1.0 mM for the metal complexes and 0.10 M for the supporting electrolyte, (*n*-Bu_4N PF_6. The addition of Et_3NHCl (0.1 mM in CH_3CN) was carried out with syringe.[61]

Photoinduced hydrogen evolution was performed in a 40 mL flask. The flask was sealed with a septum, pre-degassed by bubbling N_2 for 15 min under atmospheric pressure at room temperature. In the experiment of varying amounts of the catalyst, the 1:1 EtOH/H_2O solution containing **Fl** and TEA were added with the total volume of 5.0 mL. The pH of the solution was adjusted to a suitable pH by adding HCl or NaOH and was measured by the pH meter. Then the samples were irradiated by a 500 W Xenon lamp with a 400 nm filter to ensure the excitation of the photosensitizer only. The reaction temperature was 293 K by using a water filter to absorb heat. The generated photoproduct of H_2 was characterized by GC 7890T instrument analysis using a 5Å molecular sieve column(0.6 m× 3.0mm), thermal conductivity detector, and nitrogen used as carrier gas. The amount of H_2 generated was determined by the external standard method. Hydrogen in the resulting solution was not measured and the slight effect of the hydrogen gas generated on the pressure of the flask was neglected for calculation of the volume of hydrogen gas.[37]

Syntheses and Characterizations.

2-(2-diphenylphosphino)benzylidenehydrazinecarbothio amide (HthioP): 2-(diphenylphosphino)benzaldehyde (0.58g, 2mmol) and thiosemicarbazone (0.20g, 2.2 mmol) were mixed in 25 mL methanol. After refluxing for 4 h, a yellow solid formed which was isolated, washed with methanol and dried under vacuum. 0.57g product was obtained with yield of 78%. Anal. Calc. for $C_{20}H_{18}N_3SP$: H, 4.99; C, 66.1; N, 11.56. Found: H, 5.04; C, 65.69; N, 11.50. ^{1}H NMR (DMSO-d_6, 400MHz ppm): 11.57 (s, 1H, N(H)S), 8.69 (d, 1H, H4, J = 7.2 Hz), 8.20 (t, 2H, NH_2), 7.75 (s, 1H, H_5), 7.43(m, 7H, H_α, H_γ, H1), 7.33 (t, 1H, H_3 J = 7.2Hz), 7.19 (m, 4H, H_β, J = 4.2 Hz), 6.77 (t, 1H, H_2, J = 7.2 Hz); API-MS *m/z:* 363.1 ([M+H$^+$]).

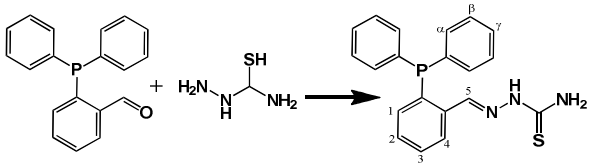

Co–thioP:2-(2-(diphenylphosphino)benzylidene)hydrazinecarbo-thioamide (0.22 g, 0.6 mmol) and cobalt(II) ditetra-fluoroborate (0.10g, 0.3 mmol) were mixed in 10 mL methanol. After refluxing for 2 h, the solvent was allowed to cool to room temperature; stand in air at room temperature for several days, black crystals obtained dried under vacuum. 0.21g product was obtained with yield of 75 %. Anal. calcd. for $C_{40}H_{35}N_6P_2S_2CoBF_4{\cdot}2H_2O$(%): C 52.91, H 4.33, N 9.26; Found: C: 53.33; H 3.79; N 9.32. ^{1}H NMR (MeOD, 400MHz ppm): 8.57 (d, 1H, H_4, J= 7.2 Hz), 7.93 (t, 2H, NH_2), 7.64 (s, 1H, H_5), 7.44 (m, 7H, H_α, H_γ, H_1), 7.39 (t, 1H, H_3 J = 7.2Hz), 7.22 (m, 4H, H_β, J = 4.2 Hz), 6.86 (t, 1H, H_2, J = 7.2 Hz); ESI-MS *m/z*: 783.18 for the +1 charge cation.

Ni–thioP:2-(2-(diphenylphosphino)benzylidene) hydrazinecarbo-thioamide (0.22 g, 0.6 mmol) and nickel(II) ditetra- fluoroborate hexahydrate (0.10g, 0.3mmol) were mixed in 10 mL methanol. After refluxing for 2 h, the solvent was allowed to cool to room temperature; stand in air for several days, pink crystals obtained were dried under vacuum. 0.22g product was obtained with yield of 80%. Anal. calcd. for $C_{40}H_{35}N_6OP_2S_2Ni{\cdot}$ $BF_4{\cdot}H_2O$: C, 53.01; H, 4.12; N, 9.28; Found. C 52.94, H 3.98, N 9.53, ^{1}H NMR (CD_3CN, 400MHz ppm): 10.68 (*s*, 1H, NH_2), 10.35 (*s*, 1H, NH_2), 8.71 (*s*, 2H, NH2) 8.58 (s, 1H, H_5), 8.05 (m, 1H, H_4'), 8.01 (m, 1H, H_4), 7.69 (m, 7H, H_α, H_γ, H_1), 7.53(m, 8H, H_α', $H_{\gamma'}$, $H_{1'}$, $H_{5'}$), 7.43 (m, 5H, $H_{\beta'}$, $H_{3'}$), 7.39 (m, 1H, H_3), 7.30 (m, 4H, H_β), 7.18 (m, 1H, $H_{2'}$); 6.95 (m, 1H, H_2). ESI-MS *m/z*: 799.29 for the +1 charge cation.

Crystallographic Data for Co-thiop and Ni-thiop

Intensities were collected on a Bruker SMART APEX CCD diffrac- tometer with graphite-monochromated Mo-Kα(λ = 0.71073 Å) using the SMART and SAINT programs.[62] The

structures were solved by direct methods and refined on F^2 by full-matrix least-squares methods with SHELXTL version 5.1.[63] In both of the two structural refinements, except several partly occupied solvent water molecules, the non-hydrogen atoms were refined anisotropically. Hydrogen atoms within the ligand backbones were fixed geometrically at the calculated distances and allowed to ride on the parent non-hydrogen atoms, whereas no hydrogen atoms corresponding to the solvent molecules were added and refined. Three of the four fluoride atoms on the $BF4^-$ anion were disordered into two parts with the s.o.f of each part being fixed at 0.5 for Co–**thioP** or refined with free values for Ni–**thioP**, respectively.

Co–thioP: $CoC_{43}H_{53}N_6O_6P_2S_2BF_4$ Mr = 1021.71, Monoclinic, space group $P2_1/c$, red block, a = 13.320(1) Å, b = 25.238(1), c = 15.081(1), β = 109.34(1), V = 4783.5(2) Å3, Z = 4, Dc = 1.419 gcm-3, μ (Mo-Kα) = 0. 815 mm-1, T = 296(2) K. 8400 unique reflections [Rint = 0.0573]. Final R1 [with I > 2σ(I)] = 0.0608, wR_2 (all data) = 0.1812. CCDC No. 936190.

Ni–thioP: $NiC_{42}H_{47}N_6O_5P_2S_2BF_4$ Mr = 987.44, Triclinic, space group P-1, red block, a = 9.430(1) Å, b = 12.855(1), c = 21.767(2), α = 93.41(1), β = 91.48(1), γ = 111.22 (1), V = 2452.3(3) Å3, Z = 2, Dc = 1.337 g cm^{-3}, μ(Mo-Kα) = 0.608 mm^{-1}, T = 296(2) K. 8612 unique reflections [R_{int} = 0.0374]. Final R_1 [with I > 2σ(I)] = 0.0678, wR_2 (all data) = 0.2176. CCDC No. 936191.

Theoretical Methods

All *ab* initio electronic structure calculations were performed using the Gaussian 09 package. The structural optimizations of complex in vacuum and the aqueous solution were done at ωB97XD/6-31+g(d,p)/LANL2DZ level. Solvent environment was treated with CPCM model. Calculation at this level is known to well reproduce the CCSD(T)/CBS level results of π-π stacking of aromatic molecules. The experimental structure of Ni–thioP was well reproduced by the DFT calculations with ωB97XD functional. Extensive density functional theory (DFT)-based calculations were also performed to prove the aforementioned reaction mechanism for proton reduction.

Acknowledgments

We acknowledge the financial support from the National Nature Science Fundation of China (Nos. 21273027 and 21025102) and the Program for Changjiang Scholars and Innovative Research Team in University (IRT1213).

Notes and references

[a] *State Key Laboratory of Fine Chemicals, Dalian University of Technology, Dalian, 116023, P. R. China E-mail: hecheng@dlut.edu.cn*

† Electronic Supplementary Information (ESI) available: Crystal data (CIF file), experimental details, Tables and Figures are available free of charge *via* the Internet at http://www.rsc.org.

(1) T. R. Cook, D. K. Dogutan, S. Y. Reece, Y. Surendranath, T. S. Teets and D. G. Nocera, *Chem. Rev.* 2010, **110**, 6474–6502.
(2) A. J. Bard and M. A. Fox, *Acc. Chem. Res.* 1995, **28**, 141–145.
(3) X. Chen, L. Liu, P. Y. Yu and S. Mao, *Science* 2011, **331**, 746–750.
(4) F. Wang, W. G. Wang, X. J. Wang, H. Y. Wang, C. H. Tung and L. Z. Wu, Angew. Chem. Int. Ed. 2011, **50**, 3193–3197.
(5) A. D. Yuhas, A. L. Smeigh, A. P. Douvalis, M. R. Wasielewski and M. G. Kanatzidis, *J. Am. Chem. Soc.* 2012, **134**, 10353−10356.
(6) A. R. Dismukes, G. A. Brimblecombe, N. Felton, R. S. Pryadun, J. E. Sheats, L. Spiccia and G. F. Swiegers, *Acc. Chem. Res.* 2009, **42**, 1935– 1943.
(7) R. D. Richardson, E. J. Holland and B. K. Carpenter, *Nat. Chem.* 2011, **3**, 301–303.
(8) J. Esswein and D. G. Nocera, *Chem. Rev.* 2007, **107**, 4022–4047.
(9) G. M. Brown, B. S. Brunschwig, C. Creutz, J. F. Endicott and N. Sutin, *J. Am. Chem. Soc.* 1979, **101**, 1298–1300.
(10) J. F. Dong, M. Wang, P. Zhang, S. Q. Yang, J. Y. Liu, X. Q. Li and L. C. Sun, *J. Phys. Chem., C* 2011, **115**, 15089–15096.
(11) W. Zhang, J. H. Hong, J. W. Zheng, Z. Y. Huang, J. R. Zhou and R. Xu, *J. Am. Chem. Soc.* 2011, **133**, 20680−20683.
(12) T. M. McCormick, B. D. Calitree, A. Orchard, N. D. Kraut, F. V. Bright, M. R. Detty and R. Eisenberg, *J. Am. Chem. Soc.* 2010, **132**, 15480–15483.
(13) Z. Han, W. R. Mcnamara, M. Eum, P. L. Holland and R. Eisenberg, *Angew. Chem. Int. Ed.* 2012, **51**, 1667−1670.
(14) T. S. Lobana, R. S harma, G. Bawa and S. Khanna, *Coord. Chem. Rev.* 2009, **253**, 977–1055.
(15) H. Beraldo and D. Gambino, *Mini. Rev. Med. Chem*. 2004, **4**,31–39.
(16) M. N. M. Milunovic, E. A. Enyedy, N. V. Nagy, T. Kiss, R. Trondl, M. A. Jakupec, B. K. Keppler, R. Krachler, G. Novitchi and V. B. Arion, *Inorg. Chem.* 2012, **51**, 9309−9321.
(17) H. Peng, G. F. Liu, L. Liu and D. Z. Jia, *Tetrahedron* 2005, **61**, 5926–5932.
(18) M. A. Ali, P. V. Bernhardt, M. A. H. Brax, J. England, A. J. Farlow, G. R. Hanson, L. L. Yeng, A. H. Mirza and K. Wieghardt, *Inorg. Chem.* 2013, **52**, 1650−1657.
(19) T. M. Chang and E. Tomat, *Dalton Trans.* 2013, **42**, 7846–7849.
(20) A. Credico, F. F. de Biani, L. Gonsalvi, A. Guerri, A. Ienco, F. Laschi, M. Peruzzini, G. Reginato, A. Rossin and P. Zanello, *Chem. Eur. J.* 2009, **15**, 11985–11998.
(21) L. Y. Zhang, L. J. Xu, X. Zhang, J. Y. Wang, J. Li, Z. N. Chen, *Inorg. Chem.* 2013, **52**, 5167−5175.
(22) Z. J. Han, L. X. Shen, W. W. Brennessel, P. L. Holland and R. Eisenberg, *J. Am. Chem. Soc.* 2013, **135**, 14659−14669.
(23) Le Goff, V. Artero, B. Jousselme, P. D. Tran, N. Guillet, R. Metaye, A. Fihri, S. Palacin and M. Fontecave, *Science* 2009, **326**,1384–1387.
(24) U. J. Kilgore, J. A. S. Roberts, D. H. Pool, A. M. Appel, M. P. Stewart, M. R. DuBois, W. G. Dougherty, W. S. Kassel, R. M. Bullock and D. L. DuBois, *J. Am. Chem. Soc.* 2011, **133**, 5861−5872.
(25) V. Artero, M. Chavarot-Kerlidou and M. Fontecave, *Angew. Chem, Int. Ed.* 2011, **50**, 7238–7266.
(26) M. L. Helm, M. P. Stewart, R. M. Bullock, M. R. Dubois and D. L. Dubois, *Science* 2011, **333**, 863–866.
(27) M. O'Hagan, W. J. Shaw, S. Raugei, S. T. Chen, J. Y. Yang, U. J. Kilgore, D. L. DuBois and R. M. Bullock, *J. Am. Chem. Soc.* 2011, **133,** 14301– 14312
(28) P. W. Du and R. Eisenberg, *Energy Environ. Sci.* 2012, **5**, 6012–6021.
(29) S. Lossea, J. G. Vosc and S. Raub, *Coord. Chem. Rev.* 2010, **254**, 2492–2504.
(30) C. J. Fang, C. Y. Duan, C. He, G. Han and Q. J. Meng, *New J. Chem.* 2000, **24** , 697−701.
(31) M. P. Stewart, M. H. Ho, S. M.Wiese, L. Lindstrom, C. E. Thogerson, S. Raugei, R. M. Bullock and M. L. Helm, *J. Am. Chem. Soc.* 2006, **128**, 358−366.
(32) M. R. Dubois, D. L. Dubois, *Acc. Chem. Res.* 2009, **42**, 1974−1982.
(33) M. O'Hagan, M. H. Ho, J. Y. Yang, A. M. Appel, M. R. R. Dubois, S. Raugei, W. J. Shaw, D. L. Dubios and R. M. Bullock, *J. Am. Chem. Soc.* 2012, **134**, 14409−14424.
(34) H. H. Cui, J. Y. Wang, M. Q. Hu, C. B. Ma, H. M. Wen, X. W. Song and C. N. Chen, *Dalton Trans.* 2013, **42**, 8684–8691.
(35) H. N. Kagalwala, E. Gottlieb, G. Li, T. Li, R. C. Jin, S. Bernhard, *Inorg. Chem.* 2013, **52**, 9094−9101.
(36) R. Cowley, J. R. Dilworth, P. S. Donnelly, E. Labisbal, A. Sousa *J. Am. Chem. Soc.* 2002, **124**, 5270–5271.
(37) L. Petrou, A. D. Koutselos, H. S. Wahab, W. Clegg, R. W. Harrington and R. A. Henderson, *Inorg. Chem.* 2011, **50**, 847−857.

(38) M. Ohangan, M. H. Ho, J. Y. Yang, A. M. Appel, M. R. Dubois, S. Raugei, W. J. Shaw, D. L. Dubois and R. M. Bullock, *J. Am. Chem. Soc.* **2012**, *134*, 19409−19424.

(39) M. R. Dubois and D. L. DuBois, *Chem. Soc. Rev.* 2009, **38**, 62–72.

(40) J. M. Camara and T. B. Rauchfuss, *J. Am. Chem. Soc.* 2011, **133**, 8098− 8101.

(41) M. Wang, L. Chen, X. Q. Li and L. C. Sun, *Dalton Trans.* 2011, **40**, 12793 −12800.

(42) Hagfeldt, G. Boschloo, L. C. Sun, L. Kloo and H. Pettersson, *Chem. Rev.* 2010, **110**, 6595−6663.

(43) P. D. Frischmann, K. Mahata, F. Würthner, *Chem. Soc. Rev.* 2013, **42**, 1847−1870.

(44) G. W. Frisch, H. B. Schlegel, G. E. Scuseria, M. A. Robb, J. R. Cheeseman, G. Scalmani, V. Barone, B. Mennucci, G. A. Petersson, H. Nakatsuji, M. Caricato, X. Li, H. P. Hratchian, A. F. Izmaylov, J. Bloino, G. Zheng, J. L. Sonnenberg, M. Hada, M. Ehara, K. Toyota, R. Fukuda, J. Hasegawa, M. Ishida, T. Nakajima, Y. Honda, O. Kitao, H. Nakai, T. Vreven, Jr. J. A. Montgomery, J. E. Peralta, F. Ogliaro, M. Bearpark, J. J. Heyd, E. Brothers, K. N. Kudin, V. N. Staroverov, R. Kobayashi, J. Normand, K. Raghavachari, A. Rendell, J. C. Burant, S. S. Iyengar, J. Tomasi, M. Cossi, N. Rega, J. M. Millam, M. Klene, J. E. Knox, J. B. Cross, V. Bakken, C. Adamo, J. Jaramillo, R. Gomperts, R. E. Stratmann, O. Yazyev, A. J. Austin, R. Cammi, C. Pomelli, J. W. Ochterski, R. L. Martin, K. Morokuma, V. G. Zakrzewski, G. A. Voth, P. Salvador, J. J. Dannenberg, S. Dapprich, A.D. Daniels, Ö. Farkas, J. B. Foresman, J. V. Ortiz, J. Cioslowski and D. J. Fox, *Gaussian 09W, revision A01*; Gaussian, Inc.: Wallingford CT, 2009.

(45) Y. Zhao, X. Liu, K. X. Yao, L. Zhao and Y. Han, *Chem. Mat.,* 2012, *24*, 4725–4734

(46) X. B. Chen, C. Li, M. Gratzer, R. Kostechi and S. S. Mao, *Chem. Soc*. *Rev*., 2012, **41**, 7909–7937.

(47) F. E. Osterloh, *Chem. Soc. Rev.*, 2013, **42**, 2249-2320.

(48) C. Y. Duan, Z. H. Liu, X. Z. You, F. Xu and T. C. W. Mak, *Chem. Commun.* 1997, 381–382.

(49) M. X. Li, C. L. Chen, D. Zhang, J. Y. Niu and B. S. Ji, Eur. J. Med. Chem. 45 (2010) 3169–3177

(50) K. V. Katti, P. R. Singh and C. L. Barnes, J. Chem. Soc., Dalton Trans. (1993) 2153–2159.

(51) Y. G. Zhao, D. Guo, Y. Liu, C. He and C. Y. Duan, *Chem. Commun.* 2008, 5725–5727.

(52) M. P. Stewart, M. H. Ho, S. Wiese, M. L. Lindstrom, C. E. Thogerson, S. Raugei, R. M. Bullock and M. L. Helm, *J. Am. Chem. Soc.* 2013, **135**, 6033−6046.

(53) M. Razavet, V. Artero and M. Fontecave, *Inorg. Chem.* 2005, **44**, 4786− 4795.

(54) H. I. Kasunadasa, C. J. Chang and J. R. Long, *Nature* 2010, **464**, 1329− 1333.

(55) T. Lazarides, T. McCormick, P. W. Du, G. G. Luo, B. Lindley, R. Eisenberg, *J. Am. Chem. Soc.* 2009, **131**, 9192–9194.

(56) P. Zhang, M. Wang, Y. Na, X. Q. Li, Y. Jiang and L. C. Sun, *Dalton Trans.* 2010, **39**, 1204–1206

(57) W. R. McNamara, Z. Han, P. J. Alperin,W. Brennessel, P. L. Holland and R. Eisenberg, *J. Am. Chem. Soc.* 2011, **133**, 15368− 15371.

(58) W. R. McNamara, Z. J. Han, C. J. Yin, W. W. Brennessel, P. L. Holland and R. Eisenberg *Proc. Natl. Acad. Sci. USA.* 2012, **109**, 15595−15599.

(59) P. Zhang, M. Wang, J. Dong, X. Li, F. Wang, L. Wu and L. C. Sun, J. Phys. Chem. C 2010, **114**, 15868–15874.

(60) L. Li, L. L. Duan, F. Y. Wen, C. Li, M. Wang, A. Hagfeldt and L. C. Sun, *Chem. Commun.* 2012, **48**, 988−990.

(61) M. Razavet, V. Artero and M. Fontecave, *Inorg. Chem.* 2005, **44** 4786 −4795

(62) SMART and SAINT,Area Detector Control and Integration Software; Siemens Analytical X-ray Systems, Inc.: Madison, WI, 1996.

(63) G. M. Sheldrick, SHELXTL V5.1, Software Reference Manual; Bruker, AXS, Inc.: Madison, WI, 1997.